Environmental Pollution 254 (2019) 112864

Contents lists available at ScienceDirect

Environmental Pollution

journal homepage: www.elsevier.com/locate/envpol

Chemistry-triggered events of $PM_{2.5}$ explosive growth during late autumn and winter in Shanghai, China☆

Wenwen Sun [a], Dongfang Wang [b], Lan Yao [a], Hongbo Fu [a], Qingyan Fu [b], Hongli Wang [c], Qing Li [a], Lin Wang [a], Xin Yang [a], Aiyong Xian [d], Gehui Wang [e], Hang Xiao [f], Jianmin Chen [a, e, f, *]

[a] Shanghai Key Laboratory of Atmospheric Particle Pollution and Prevention, Department of Environmental Science & Engineering, Institute of Atmospheric Sciences, Fudan University, Shanghai 200438, China
[b] Shanghai Environmental Monitoring Center, Shanghai 200235, China
[c] Shanghai Academy of Environmental Sciences, Shanghai 200233, China
[d] Yellow River Shandong Bureau, Jinan 250000, China
[e] Institute of Eco-Chongming, 3663 Zhongshan Road, Shanghai 200062, China
[f] Center for Excellence in Regional Atmospheric Environment, Institute of Urban Environment, Chinese Academy of Sciences, Xiamen 361021, China

ARTICLE INFO

Article history:
Received 2 April 2019
Received in revised form
3 July 2019
Accepted 6 July 2019
Available online 18 July 2019

Keywords:
$PM_{2.5}$
Chemical composition
Secondary formation
Primary emission

ABSTRACT

To better understand the mechanism of $PM_{2.5}$ explosive growth (EG), we conducted concurrent measurements of gaseous pollutants, $PM_{2.5}$ and its chemical composition (inorganic ions, organic carbon, and element carbon) with a time resolution of 1 h in Shanghai in late autumn and winter from 2014 to 2017. In this study, the EG events, which are defined as the net increase in the mass concentration of $PM_{2.5}$ by more than 100 $\mu g\,m^{-3}$ within hours, are separately discussed for 3, 6, or 9 h. The number of EG events decreased from 19 cases in 2014 to 6 cases in 2017 and the corresponding $PM_{2.5}$ concentration on average decreased from 183.6 $\mu g\,m^{-3}$ to 128.8 $\mu g\,m^{-3}$. Both regional transport and stagnant weather (windspeed < 2.0 $m\,s^{-1}$) could lead to EG events. The potential source contribution function (PSCF) shows that the major high-pollution region is in East China (including Zhejiang, Jiangsu, Shandong, and Anhui Province) and the North China Plain. The contribution of stagnant conditions to EG episode hours of 55% (198 h, 156.9 $\mu g\,m^{-3}$) is higher than that of regional transport (45%, 230 h, 163.0 $\mu g\,m^{-3}$). To study the impact of local emission, chemical characteristics and driving factors of EG were discussed under stagnant conditions. The major components contributing to $PM_{2.5}$ are NO_3^- (17.9%), organics (14.1%), SO_4^{2-} (13.1%), and NH_4^+ (13.1%). The driving factors of EG events are the secondary aerosol formation of sulfate and nitrate and primary emissions (vehicle emissions, fireworks, and biomass burning), but the secondary transformation contributes more to EG events. The formation of sulfate and nitrate is dominated by gas-phase oxidation and heterogeneous reactions, which are enhanced by a high relative humidity. The current study helps to understand the chemical mechanism of haze and provides a scientific basis for air pollution control in Shanghai.

1. Introduction

China suffers from severe levels of air pollution due to extremely high levels of fine particulate matter ($PM_{2.5}$), especially during the winter (Fu and Chen, 2017; Huang et al., 2014; Wang et al., 2014a). These severe haze events feature a rapid increase in the $PM_{2.5}$ mass concentration, which reaches a very high level in a short amount of time, and have been defined differently by several researchers (Ji et al., 2014; Wang et al., 2014b; Zheng et al., 2015; Zhong et al., 2018). Zheng et al. (2015) termed this phenomenon a sharp-increase event, during which the $PM_{2.5}$ concentration increases by more than 400 $\mu g\,m^{-3}$ in 1–3 h. Wang et al. (2014b) called this phenomenon an explosive growth (EG) episode, which is characterized by a very high $PM_{2.5}$ concentration that only lasts a few

☆ This Paper has been recommended for acceptance by Admir Créso Targino.

* Corresponding author. Shanghai Key Laboratory of Atmospheric Particle Pollution and Prevention, Department of Environmental Science & Engineering, Institute of Atmospheric Sciences, Fudan University, Shanghai 200438, China.
E-mail address: jmchen@fudan.edu.cn (J. Chen).

https://doi.org/10.1016/j.envpol.2019.07.032
0269-7491/

hours. When this phenomenon is longer-lasting (i.e., a few days) and has a lower peak $PM_{2.5}$ concentration than that the EG, it is called "sustained growth" (Wang et al., 2014b). Zhong et al. (2018) also called this phenomenon EG and defined it as a $PM_{2.5}$ concentration exceeding 80 $\mu g\,m^{-3}$ within three consecutive days, with peak values above 400 $\mu g\,m^{-3}$, where the concentration at least doubled within several hours (or 10 h). These events, with a maximum hourly average $PM_{2.5}$ mass concentration of 1000 $\mu g\,m^{-3}$, lead to a sharp decrease in visibility (Fu and Chen, 2017) and pose a considerable threat to human health (Zhong et al., 2018).

The major factors contributing to the formation of haze–fog events in Tianjin are the regional transport, adverse meteorological conditions, primary emissions, and secondary aerosol formation of particles (Han et al., 2014). However, the formation mechanisms of the EG of $PM_{2.5}$, which results in severe haze episodes with exceedingly high $PM_{2.5}$ concentrations in a short time, are still poorly understood. The mass concentrations and chemical constituents of $PM_{2.5}$ in Beijing remarkably vary, depending on complex mutual effects between the meteorology, atmospheric chemical processes, and pollution sources (Guo et al., 2014). The air quality in Beijing, Shanghai, Guangzhou, and Xi'an is closely related to the meteorological state, which is responsible for the regional transport and dispersion of air pollutants in the lower atmosphere (Huang et al., 2014; Zheng et al., 2015; Zhong et al., 2018). Zheng et al. (2015) compared surface meteorological factors with the $PM_{2.5}$ concentrations in several cities (Beijing, Tianjin, and Hebei) and reported that an EG episode could mainly be ascribed to regional transport in the North China Plain (NCP). In contrast, Zhong et al. (2018) used ground and vertical meteorological data in Beijing to analyze the relative contributions of meteorological factors to EG. They argued that this is occasionally unreasonable because EG might occur at weak wind speeds and stable stratification, which are unfavorable for transport. The characteristics of winter haze include stagnant conditions with a low mixing height, a high relative humidity (RH), abundant emissions of primary pollutants, and fast formation of secondary inorganic aerosols. Zhang et al. (2015) analyzed the meteorological parameters, gas precursors and gas-particle conversions under different visibility ranges over 71 big cities in eastern China. Under stagnant conditions, the quick conversion of primary gaseous pollutants to secondary aerosols greatly contributes to the EG (Fu and Chen, 2017; Huang et al., 2014; Zhang et al., 2015).

For a typical event with EG of fine particles, Wang et al. (2014b) found that organic matter, sulfate and nitrate have the largest contributions to the increase in $PM_{2.5}$. During historical regional pollution episodes, the mass ratio of secondary inorganic aerosols (SIA) is more than one third in both Beijing and Shanghai (Ji et al., 2018; Wang et al., 2015). The SIA mainly form through complex atmospheric chemical processes, including heterogeneous processes and gas-phase reaction on the particle surfaces (Ji et al., 2018; Wang et al., 2018a; Zheng et al., 2015). Field measurements have shown that nitrate and sulfate play significant roles in the growth of fine particles (Ji et al., 2018; Wang et al., 2018a; Zheng et al., 2015). The main formation pathway of a homogeneous gas-phase reaction is the oxidation of SO_2 by OH radicals to SO_3 and to H_2SO_4 (Wang et al., 2018a). The heterogeneous uptake of SO_2 by pre-existing particles or cloud droplets and the oxidation by O_3, NO_2, H_2O_2, and transition metals are also crucial for sulfate formation (Zheng et al., 2015). Under ammonia-rich conditions, nitrate mainly forms by ammonia reacting with nitric acid in droplets or gaseous HNO_3 (Ji et al., 2018). However, under ammonia-poor condition, the formation is dominated by the heterogeneous hydrolysis reaction of N_2O_5 on aerosol surfaces (Ji et al., 2018). This pathway mainly occurs at night under high RH, acidic aerosol, and low-temperature conditions (Wang et al., 2018a). During the daytime, NO_x reacts with hydroxyl radicals to produce nitric and nitrous acids through complex photochemical reactions and then combines with NH_3 to form particulate NO_3^- (Ji et al., 2018; Tian et al., 2016; Wang et al., 2018a).

Previous studies on the chemical compositions and physical characteristics during EG events mainly focused on the Beijing–Tianjin–Hebei (Jing-Jin-Ji) area (Ji et al., 2014; Wang et al., 2014b; Wang et al., 2018b; Zheng et al., 2015; Zhong et al., 2018) and few efforts have been made to understand the EG in the Yangtze River Delta (YRD; Wang et al., 2016a; Zhong et al., 2019). Stagnant weather is favorable for investigations of local emissions and the local secondary formation characteristics. Thus, it is meaningful to explore the driving factors of EG episodes under stagnant conditions to provide useful information to the government, which will enable forecasts and the reduction of severe atmospheric pollution. In this study, online measurements of the $PM_{2.5}$ mass loading, chemical components, major precursors, and major meteorological variables, were carried out during late autumn and winter in Shanghai from 2014 to 2017, to explore the factors that lead to EG events.

2. Experiment and method

2.1. Site description

The sample site is in the Qingpu Environmental Monitoring Center (Dianshanhu supersite, 31.09°N, 120.98°E) in the west suburb, 45 km from the center of Shanghai (Fig. S1, right). The Qingpu District is bordered by the Zhejiang Province in the south and the Jiangsu Province in the west. The land use types near the sampling site include a few residential areas, agriculture, factories, and highways. Shanghai is characterized by a subtropical monsoon climate, which is moderately moist, has an annual average air temperature of 8.5 °C, solar radiation duration of 121.1 h, and precipitation of 59.0 mm during late autumn and winter between 2014 and 2017. The RH in January, February, November, and December between 2014 and 2017 was 71.5%. Shanghai is generally influenced by other parts of the YRD and NCP regions; the prevailing wind direction ranges from northwest to north in winter. During the summer, it is a contributor to the other YRDs (Leng et al., 2016). The Dianshan Lake, with an area of up to 62 km^2, is 0.2 km away from the western and northern edges of the super site, which leads to a high RH at the sampling sites.

2.2. Measurements

The hourly concentrations of $PM_{2.5}$, eight types of water-soluble inorganic ions (WSIIs, including NO_3^-, SO_4^{2-}, NH_4^+, Cl^-, K^+, Na^+, Ca^{2+}, and Mg^{2+}), carbonaceous components [organic carbon (OC) and element carbon (EC)], trace gases (CO, O_3, SO_2 and NO_2), and meteorological parameters were measured online in Shanghai in January, February, November, and December from 2014 to 2017. The $PM_{2.5}$ level was measured automatically using a tapered element oscillating microbalance (TEOM 1405-D, Thermo Scientific Co., MA, USA). The flow rate of the TEOM was 16.7 L min^{-1}. The average sampling time was 5 min; it was converted to hourly means. The uncertainty of the hourly measurement is ±1.50 $\mu g\,m^{-3}$, and the detection limit is 0.06 $\mu g\,m^{-3}$. The gaseous species were continuously measured using a set of gas analyzers including an O_3 analyzer (model 49I), NO/NO_2 analyzer (model 42I), SO_2 analyzer (model 43I), and CO analyzer (model 48I; Thermo Scientific, USA). Gas data were collected every minute and converted into hourly averages. Gas analyzers of SO_2, NO_x, and CO were calibrated using standard gas with 50 ppmv SO_2, 52 ppmv NO, and 5000 ppmv CO,

respectively. The O_3 analyzer was calibrated with a special O_3 calibrator (49C PS), which was zeroed every 2 h using an internal catalytic converter. The precision of the O_3, NO/NO_2, SO_2, and CO analyzers are 1.0 ppb, 0.4 ppb, 1.0 ppb, and 0.1 ppb, respectively.

A MARGA instrument (ADI 2080, Applikon Analytical, Netherlands) equipped with a $PM_{2.5}$ sharp-cut cyclone inlet was used to detect WSIIs with a time resolution of 1 h at a flow rate of 16.7 L min^{-1}. The sample system contains two parts: a gas sample and an aerosol sample. The gas was sampled with a wet rotating denuder and the aerosol was sampled with a steam jet aerosol collector. Ion chromatography (IC, conductivity detector) was then used to analyze the two types of collected liquid samples. We used an internal calibration (bromide as anion and lithium as cation) and external standard (mixed anion and cation standards) to calibrate the MARGA. Furthermore, we performed multi-point calibrations for the soluble ions of the target water before and after the campaign. The detection limits for NO_3^-, SO_4^{2-}, Cl^-, NH_4^+, K^+, Na^+, Mg^{2+}, and Ca^{2+} are 0.05, 0.04, 0.01, 0.05, 0.09, 0.05, 0.06 and 0.1 μg m^{-3}, respectively (based on a 45 min sampling time). The detailed principles of MARGA can be found in Kong et al. (2018).

The OC and EC concentrations were analyzed online with a Sunset Semi-Continuous Carbon Analyzer (Sunset Laboratory, Forest Grove, Oregon, USA) using the thermal-optical transmittance method, and a flow rate of 8 L min^{-1}. The OC and EC data were collected every 30 min and converted into hourly averages. The organic compounds were first vaporized in pure helium. We then used the manganese dioxide oxidizing oven to oxidize them to CO_2, which was quantified by using a non-dispersive infrared detector. The EC was then oxidized with an oxygen blend carrier gas and quantified with the same method as used for the OC. The instrument was calibrated by injecting a certain volume of methane, which was oxidized and quantified as an internal standard. The results measured by this instrument and analyzed by the filter have good correlations. The precision, with a relative standard deviation below 5%, is satisfactory. To calibrate the samples, we analyzed the field blanks. The EC content can be neglected, but the OC concentration ranges from 0.1 to 1.0 μg m^{-3}. The detection limits of the OC and EC concentrations are 0.2 and 0.04 μg m^{-3}, respectively (based on a 45 min sampling time). The detailed principles of the OC/EC analyzer can be found in Tian et al. (2016). The meteorological parameters, including the RH, ambient temperature (T), wind speed (WS), and wind direction (WD), were monitored at the local automatic meteorological station, which is installed on a rooftop, 18 m above the ground. The data were collected every minute and converted to hourly means.

2.3. Explosive growth

The EG event has been defined in previous studies, which will be described briefly in this section. Wang et al. (2014b) treated a rapid increase in the $PM_{2.5}$ concentration from a low level (<35 μg m^{-3}) to an exceedingly high level (>500 μg m^{-3}) within 8 h in the Jing-Jin-Ji area as an EG episode. Following this work, Zhong et al. (2018) defined an event as EG when the mass concentration of $PM_{2.5}$ at least doubled in several hours (or 10 h) in Beijing during heavy-pollution episodes (a $PM_{2.5}$ concentration >80 μg m^{-3} for three consecutive days with a peak value > 400 μg m^{-3}). However, most of the previous studies on EG only focused on the Jing-Jin-Ji area (Ji et al., 2014; Wang et al., 2014b; Wang et al., 2018b; Zheng et al., 2015; Zhong et al., 2018) and EG events in the YRD area were rarely studied (Wang et al., 2016a; Zhong et al., 2019). Therefore, considering the typical air pollution characteristics of Shanghai, we propose our own definition of EG in 3, 6, and 9 h in this study. The EG is defined in Eq. (1):

$$\begin{array}{ll} EG\ in\ 3\ h: & \Delta PM_{2.5} \geq 100\ \mu g\ m^{-3}\ \ and\ \ 0 < \Delta t \leq 3 \\ EG\ in\ 6\ h: & \Delta PM_{2.5} \geq 100\ \mu g\ m^{-3}\ \ and\ \ 3 < \Delta t \leq 6 \\ EG\ in\ 9\ h: & \Delta PM_{2.5} \geq 100\ \mu g\ m^{-3}\ \ and\ \ 6 < \Delta t \leq 9 \end{array} \quad (1)$$

where *EG in 3 h* denotes the net increase in the $PM_{2.5}$ mass concentration by more than 100 μg m^{-3} in 3 h; *EG in 6 h* denotes the net increase in $PM_{2.5}$ by more than 100 μg m^{-3} in 6 h, excluding the increase within 3 h; and *EG in 9 h* denotes the net increase in $PM_{2.5}$ by more than 100 μg m^{-3} in 9 h, excluding the increase within 3 and 6 h.

2.4. Potential source contribution function

The Hybrid Single-Particle Lagrangian Integrated Trajectory (HYSPLIT)-4 model with a grid size of 0.5° × 0.5° was used to calculate 48 h back trajectories starting at the arrival height of 500 m above the ground level at the Dianshanhu supersite (31.09°N, 120.98°E). The National Center for Environmental Prediction's Global Data Assimilation System produced the 6-hourly final global analysis data. The model was run four times every day at 00:00, 06:00, 12:00, and 18:00 coordinated universal time (08:00, 14:00, 20:00 and 02:00 local standard time, LST, respectively) in January, February, November, and December from 2014 to 2017.

We used the potential source contribution function (PSCF) model in terms of the HYSPLIT analysis to identify the potential source area of this pollution. The area was divided into small equal grid cells of i × j. The ijth cell of the PSCF value was defined as:

$$PSCF_{(ij)} = m_{ij}/n_{ij}, \quad (2)$$

where m_{ij} denotes the "polluted" trajectory endpoint number in the *ij*th cell and n_{ij} denotes the endpoint numbers that fall in the *ij*th cell.

To reduce the influence of small n_{ij} values and avoid the uncertainties in the calculations, the annual PSCF values were multiplied by arbitrary annual weight functions $W(n_{ij})$, which can be expressed by the weighted potential source contribution function (WPSCF; Polissar et al., 1999):

$$W(n_{ij}) = \begin{cases} 1.00 & 3n_{ave} < n_{ij} \\ 0.7 & 1.5n_{ave} < n_{ij} \leq 3n_{ave} \\ 0.42 & n_{ave} < n_{ij} \leq 1.5n_{ave} \\ 0.05 & n_{ij} \leq n_{ave} \end{cases} \quad (3)$$

where n_{ave} denotes the mean number of endpoints in the grid cell. In our study, the 24 h air quality standard of $PM_{2.5}$ in China (75 μg m^{-3}) was regarded as the "pollution" threshold (Zhao et al., 2015). The dominant ranges were 20°N–55°N in latitude and 88°E–145°E in longitude. The resolution of the model in this study was 0.5° × 0.5° grid cells.

2.5. Growth rate of the chemical components

The growth rate on the surface of the chemical components was defined as follows:

$$\frac{\Delta C}{\Delta t} = \frac{\Delta C_{t+1} - \Delta C_t}{1\ hour}, \quad (4)$$

where ΔC denotes the variable quantity of the chemical components and Δt represents the time variation. Equation (4) describes the variable quantity of the concentration of chemical components in 1 h. However, this calculation method has some weaknesses; it

can be easily affected by physical conditions such as experiment errors, the emission of gaseous pollutants, and meteorological conditions. The CO is directly emitted from the combustion process and is not very reactive. In a relatively short time period, its concentration is strongly controlled by meteorological factors. Therefore, it is a good tracer to distinguish between the dominant factors that contribute to the accumulation of these pollutants (Wang et al., 2018c). Scaling the concentration of other pollutants to CO can help to reveal the influence of atmospheric physical processes on other pollutants. Consequently, we defined the following equation:

$$\frac{\Delta(C/CO)}{\Delta t} = \frac{\Delta(C/CO)_{t+1} - \Delta(C/CO)_t}{1\ \mathrm{h}} \quad (5)$$

where $\Delta(C/CO)$ represents the variable quantity of the concentration of chemical components divided by CO.

2.6. Secondary organic carbon calculation

Our OC has two parts: primary organic carbon (POC, which is emitted directly from the particle phase) and secondary organic carbon (SOC, which is formed from gas-particle conversion; Choi et al., 2012). We calculated the POC and SOC using the minimum OC/EC ratio method (He et al., 2018), as shown in the following equations:

$$\mathrm{POC} = \mathrm{EC} \times (\mathrm{OC/EC})\mathrm{min} \quad (6)$$

$$\mathrm{SOC} = \mathrm{OC} - \mathrm{POC} \quad (7)$$

The minimum OC/EC ratio calculated using the mean of lowest 5% value is 1.09 in late autumn and winter between 2014 and 2017.

3. Results and discussion

3.1. Overview of an explosive growth episode

An EG event triggers severe haze episodes in a short amount of time with an exceedingly high level of $PM_{2.5}$, which has recently made EG a very popular topic. The EG events in 3, 6, and 9 h are shown in Fig. 1. The frequencies of the EG events were 19, 20, 6, and 6 from 2014 to 2017, respectively. There were 9 events in 3 h, 22 events in 6 h, and 20 events in 9 h. These results suggest that the annual frequency of EG gradually decreased over this period. In addition, the number of 6 and 9 h EG events is much higher than that of 3 h events. The mean levels of $PM_{2.5}$ during EG also show an annual decrease from 183.6 to 128.8 $\mu g\ m^{-3}$ between 2014 and 2017. The mean $PM_{2.5}$ concentrations decreased from 193.4 $\mu g\ m^{-3}$ in 3 h–168.5 $\mu g\ m^{-3}$ in 6 h and to 149.6 $\mu g\ m^{-3}$ in 9 h between 2014 and 2017, which were higher than those in Beijing ($143 \pm 104\ \mu g\ m^{-3}$ in 2013; Tao et al., 2015) and the Pearl River Delta (55.5–63.5 $\mu g\ m^{-3}$; Tao et al., 2017). The level of $PM_{2.5}$ gradually decreases with increasing EG duration. The EG rate of $PM_{2.5}$ shows that the EG rate at 3 h (34–41 $\mu g\ m^{-3}\ h^{-1}$) is 2.5–3.0 times faster than that at 6 h (15–24 $\mu g\ m^{-3}\ h^{-1}$) and 2.7–3.7 times faster than that at 9 h (10–13 $\mu g\ m^{-3}\ h^{-1}$; Table 1). It has been suggested that the fast EG rate can be attributed to the regional transport and local chemical production in Beijing (Wang et al., 2014b; Zheng et al., 2015). Therefore, the major frequency contributions of the regional transport to EG at 3 h (frequency: 6 cases, accounting for 67%) and stagnant weather to EG at 9 h (frequency: 13 cases, accounting for 65%; Fig. 2) indicate that most of the relatively fast EG is due to regional transport. This is described in more detail in Section 3.2. Accordingly, these EG events may be closely related to both regional transport and stagnant conditions.

3.2. Explosive growth episodes originating from stagnant conditions and regional transport

It has previously been shown that regional transport during Beijing haze pollution contributes ~56% to $PM_{2.5}$ (Li and Han, 2016). Li et al. (2015) also showed that the contributions of long-range transport to $PM_{2.5}$ in Shanghai and Suzhou were 37% and 44%, respectively, during the extremely severe haze event in January 2013. These results indicate that regional transport plays an important role in severe haze events. However, some studies suggested that stagnant conditions in winter with a low mixing height, high RH, large primary emissions, and fast secondary transformation significantly contribute to EG events (Cheng et al., 2016; Huang et al., 2017). Therefore, this section discusses EG caused by both stagnant conditions and regional transport.

Previous studies showed that a WS below 2 $m\ s^{-1}$ creates stagnant conditions (Chang et al., 2017; Giorio et al., 2015; Huang et al., 2017) and promotes the pollution due to primary emissions from road traffic to oxidize into secondary aerosols (Giorio et al., 2015). Accordingly, we define stagnant conditions as conditions with WS between 0 and 2 $m\ s^{-1}$. In contrast, a WS above 2 $m\ s^{-1}$ is treated as regional transport. The frequencies of EG events under stagnant conditions and regional transport in Shanghai during 2014–2017 are plotted in Fig. 2. The results suggest that the contributions to EG hours by regional transport and stagnant conditions were 45% and 55%, respectively. The PSCF results show that the major contributors to $PM_{2.5}$ in Shanghai are East China (including Zhejiang, Jiangsu, Shandong, and Anhui Province) and the NCP (Fig. S2 a–d). Previous studies reported that parts of the Jiangsu and Shandong provinces suffer from serious air pollution problems (Tian et al., 2016). Consequently, some of this pollution can be transported to Shanghai via air masses. However, the Yellow and the East China seas contribute relatively little to $PM_{2.5}$.

The total duration and $PM_{2.5}$ concentration of EG events under stagnant conditions (230 h, $PM_{2.5}$: 163.0 $\mu g\ m^{-3}$) are higher than those influenced by regional transport (198 h, $PM_{2.5}$: 156.9 $\mu g\ m^{-3}$). The frequency of EG events under stagnant conditions (26) is slightly higher than that based on regional transport (25; Fig. 2). Accordingly, our results provide compelling evidence that stagnant conditions are crucial for these EG events. The frequencies of EG events were 12, 7, 4, and 3 under stagnant conditions and 7, 13, 2, and 3 based on regional transport from 2014 to 2017, respectively. The frequencies of EG events under both stagnant conditions and regional transport gradually decreased over this time period, indicating an annual improvement of the air quality. Furthermore, the frequency of 3 and 6 h EG events decreased remarkably, but that of 9 h events only slightly decreased under stagnant conditions. However, there was a gradual increase in 3 h events and apparent decreases in 6 and 9 h events for regional transport during 2014–2017 (Fig. 2). The results indicate that the duration of the stagnation increased but the regional transport duration gradually shortened in Shanghai. The next section discusses EG events under stagnant conditions to understand the primary emission and formation characteristics of local pollution.

3.3. Chemical characteristics of $PM_{2.5}$ under stagnant conditions

Stagnant conditions with a low mixing height and low WS inhibit the diffusion of local pollutants, which makes them favorable for the study of local emissions, local pollution formation characteristics, and dominant sources of EG events to provide insights into the influence of stagnant conditions on EG episodes. The contributions of WSIIs and carbonaceous species to $PM_{2.5}$ are illustrated in Fig. 3. During EG events, the major components of $PM_{2.5}$ were NO_3^-, organic matter (OM, obtained by multiplying OC

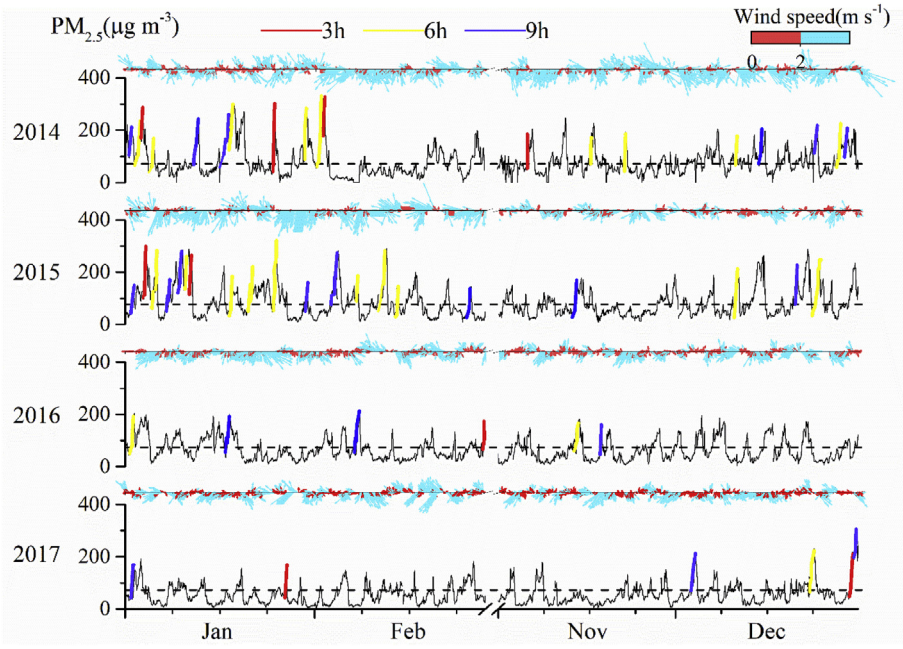

Fig. 1. Time series of $PM_{2.5}$ (the dashed lines indicate a mass concentration of 75 μg m^{-3}), WS, and WD (note that northerly and easterly wind is denoted by 0° and 90°, respectively) for Shanghai in late autumn and winter during 2014–2017. Note that the colored lines show different pollution conditions: the red, yellow, and blue lines denote an EG event of 3, 6, and 9 h, respectively; the red and cyan lines denote WDs below and above 2 m s^{-1}, respectively. (For interpretation of the references to color in this figure legend, the reader is referred to the Web version of this article.)

Table 1
Monthly averaged EG rates of $PM_{2.5}$ at 3, 6, and 9 h for Shanghai in late autumn and winter from 2014 to 2017. Note that the short line denotes that this month did not have an EG episode.

EG rate/μg $m^{-3}\cdot h^{-1}$	3 h				6 h				9 h			
	Jan	Feb	Nov	Dec	Jan	Feb	Nov	Dec	Jan	Feb	Nov	Dec
2014	40.6	36.8	37.3	–	17.5	24	19.4	15.4	10.9	–	–	11.4
2015	37.3	–	–	40.7	18.4	17.2	–	16.6	12.0	11.9	12.7	10.9
2016	–	36.3	–	–	16.2	–	16.4	–	11.4	12.4	11.7	–
2017	36.7	–	–	34.3	–	–	–	17	11.6	–	–	11.1

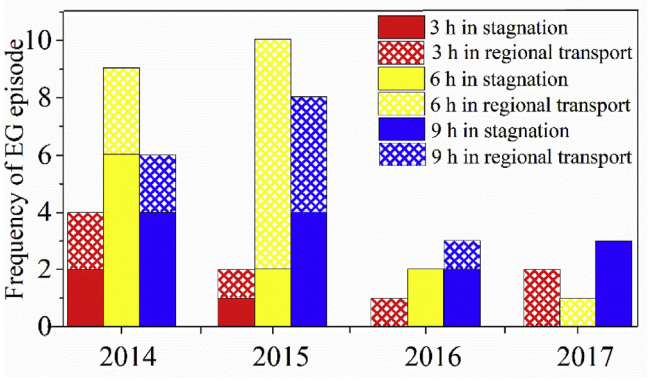

Fig. 2. Frequency of the 3, 6, and 9 h EG episodes in Shanghai in late autumn and winter from 2014 to 2017.

by a factor of 1.8; Zhou et al., 2017; Tao et al., 2015), SO_4^{2-}, and NH_4^+, accounting for 17.9%, 14.1%, 13.1%, and 13.1% from 2014 to 2017, respectively. These contributions are higher than those of NO_3^- (11.7%), SO_4^{2-} (7.7%), and NH_4^+ (6.7%) in Shanghai reported in a previous study (Leng et al., 2016). The higher contribution in this study could be due to the lower contribution of OM during 2014–2017 compared with the previous reports (Fu and Chen, 2017; Leng et al., 2016). This result indicates that the annual contribution of secondary water-soluble inorganic ions increased gradually. Furthermore, the contribution sequence of each component is inconsistent with that of Beijing, OM (31.2%) > NO_3^- (19.0%) > SO_4^{2-} (14.7%) > NH_4^+ (10.3%; Ye et al., 2017), and Suzhou, OC (20%) > SO_4^{2-} (17%) > NH_4^+ (12%) > NO_3^- (8%; Tian et al., 2016). Our results demonstrate that the role of secondary inorganic ions, especially NO_3^-, is more crucial in Shanghai than in other cities. The EG rates of NO_3^-, SO_4^{2-}, and NH_4^+ (SNA) and carbonaceous aerosol between 2014 and 2017 are illustrated in Fig. 4 and Table S1. The EG rate of the $PM_{2.5}$ components from 2014 to 2017 were: NO_3^- (3.8 μg m^{-3} h^{-1}), NH_4^+ (3.1 μg m^{-3} h^{-1}), SO_4^{2-} (2.5 μg m^{-3} h^{-1}), OM (2.1 μg m^{-3} h^{-1}), and EC (0.46 μg m^{-3} h^{-1}). The SNA EG rate was faster than that of carbonaceous compounds, which also shows that the EG is dominated by secondary inorganic compounds.

Generally, the mass ratio of NO_3^-/SO_4^{2-} is used to indicate the relative importance of mobile and stationary sources in the atmosphere (Arimoto et al., 1996). The NO_3^-/SO_4^{2-} ratio in this study is 1.5, which is dramatically higher than that in Suzhou (0.59). The sampling station in Suzhou is 300 m away from the western Nanyuan South Road and 360 m away from the northern South Ring Road Elevated Bridge. The site is a typical urban residential and commercial area, without industrial sources nearby, 40 km west of Shanghai (Tian et al., 2016). The NO_3^-/SO_4^{2-} ratio in 25% of the worst visibility periods (1.36) is higher than that in the 25% best visibility periods (1.24). This indicates that vehicle emissions may play an important role in EG events. This result is consistent with that for Guangzhou, where the NO_3^-/SO_4^{2-} ratio is 0.55 on normal days and

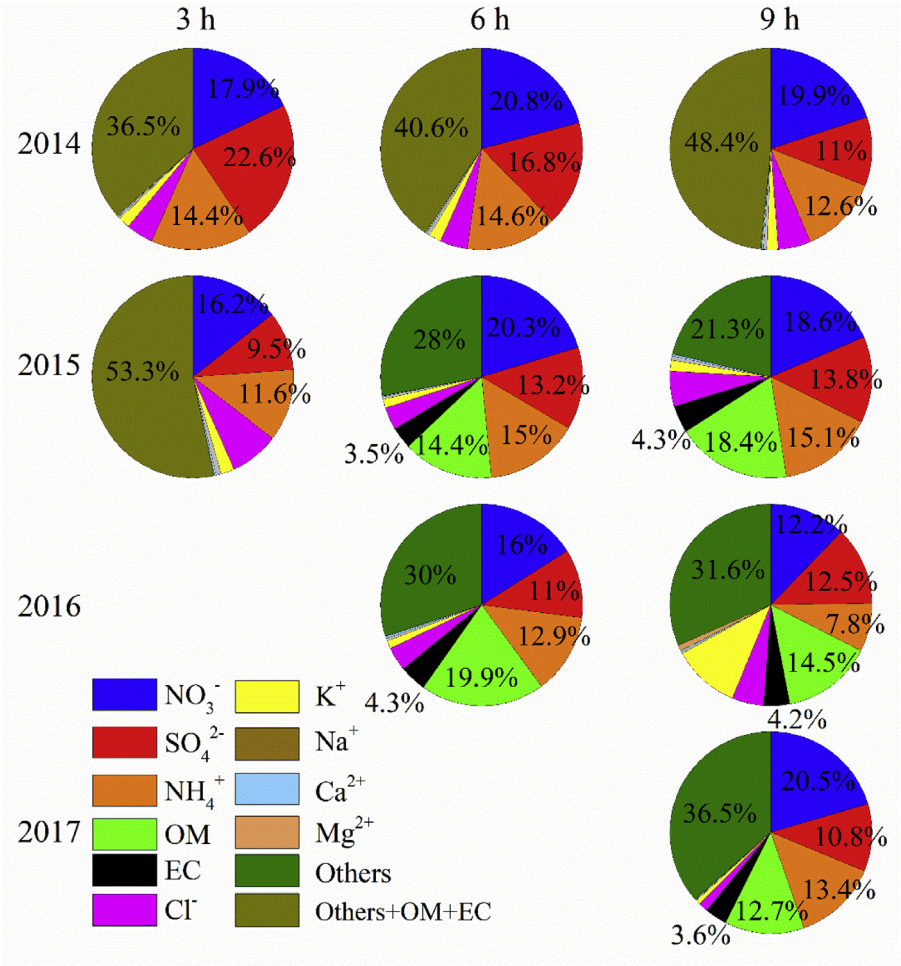

Fig. 3. Percentages of the main chemical $PM_{2.5}$ components for 3, 6 and 9 h EG under stagnant conditions in Shanghai in late autumn and winter from 2014 to 2017. Note that the dark yellow color in the pie chart includes other, OM, and EC, while the olive color only includes other because of the missing data during that period. (For interpretation of the references to color in this figure legend, the reader is referred to the Web version of this article.)

1.02 under stagnation (Tan et al., 2009). The mean ratio of the EG rate, r (NO_3^-)/r (SO_4^{2-}), is 1.6, which further verifies that the EG is dominated by mobile sources.

The average mass concentrations of WSIIs for 3, 6, and 9 h are 141.5, 96.2, and 80.8 μg m^{-3}, respectively, accounting for an average of 56% of $PM_{2.5}$, which is higher than that in Beijing (69.4 ± 55.8 μg m^{-3}, accounting for 43% of $PM_{2.5}$; Tao et al., 2015) and Suzhou (48.8 ± 24.6 μg m^{-3}, accounting for 40% in $PM_{2.5}$; Tian et al., 2016). This suggests that WSIIs play an important role in the $PM_{2.5}$ concentration in Shanghai. The average contribution of SNA to WSIIs is 85.2%, which is lower than that in Suzhou (93%; Tian et al., 2016) and Beijing (91.5%; Tao et al., 2015). The contributions of primary ions to WSIIs are: Cl^- (8.8%), followed by K^+ (4.4%), Na^+ (0.87%), Ca^{2+} (0.43%), and Mg^{2+} (0.27%). They are higher than those in Beijing: Cl^- (4.1%), K^+ (3.1%), Na^+ (0.7%), Ca^{2+} (0.4%), and Mg^{2+} (0.14%; Tao et al., 2015). These results indicate that primary emission played a more vital role during EG in Shanghai than in other cities, which is consistent with the results of Xu et al. (2018). The EG rates of NO_3^- and SO_4^{2-} exhibit trends similar to the secondary transformation rates of nitrogen (NOR) and sulfur (SOR), respectively. Both EG rates gradually decreased at 3 and 6 h but increased at 9 h between 2014 and 2017. This suggests that the secondary transformation rate gradually increased under stagnant conditions. Due to the influence of fireworks, high contributions of K^+ and Cl^- can be observed in the pie chart of EG for 6 h in 2016, which is described in more detail in the next section.

The average mass concentration of OC (14.7 ± 5.6 μg m^{-3}) is 2.4 times higher than that of EC (6.6 ± 3.3 μg m^{-3}) but lower than that obtained for Suzhou (OC is 3–29 times higher than EC; Tian et al., 2016) and Beijing (OC was 3.7 times higher than EC; Tao et al., 2015). The estimated mass concentration of SOC is 7.3 μg m^{-3}, which accounts for 50% of OC. The contribution is lower than that in Suzhou (65%; Tian et al., 2016), but higher than that in Nanjing (26%–34%; Chen et al., 2017) and Beijing (28%; Zheng et al., 2015). Another promising finding is that primary emission and secondary transformation play an equivalent role to carbonaceous species under stagnant conditions.

3.4. Case study of a typical explosive growth episode

The 3 h EG episode is driven by secondary aerosol pollution (Figs. S3 and S4). The 9 h EG episode is driven by secondary aerosol pollution and fireworks displays (Figs. S5 and S6). The 6 h EG episode is driven by secondary aerosol pollution, including nitrate (Ep1 and Ep10), sulfate (Ep2 and Ep5), and nitrate–sulfate complexes (Ep6, Ep8 and Ep9); and primary pollutants, including fireworks displays (Ep3 and Ep4) and biomass burning (BB; Ep7; Figs. 5 and 6). To understand the formation mechanism, a 6 h EG episode was used as a typical case.

The NO_3^-/SO_4^{2-} mean mass ratio in Shanghai was 1.5 in late autumn and winter between 2014 and 2017, which is similar to the results of Leng et al. (2016) for Shanghai (1.53). Consequently, we

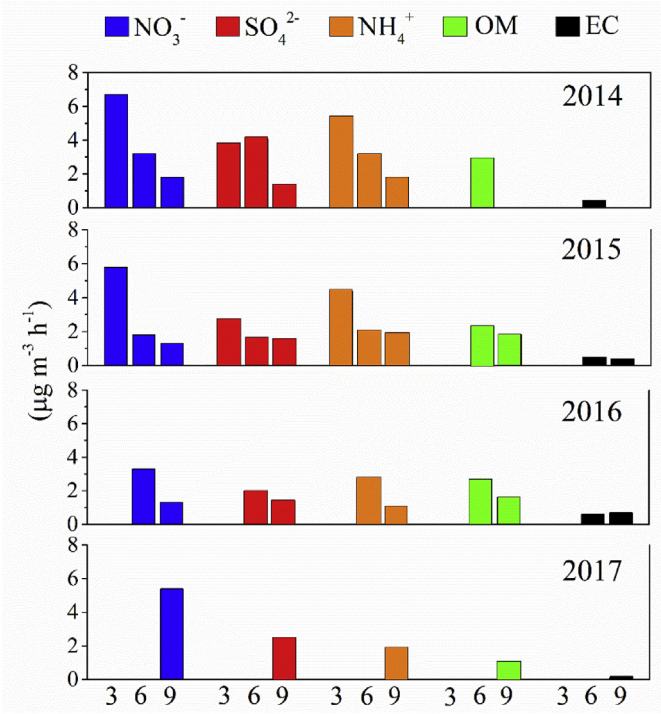

Fig. 4. EG rates of SNA, OM, and EC in Shanghai under stagnant conditions in late autumn and winter from 2014 to 2017.

defined a NO_3^-/SO_4^{2-} ratio below 1.5 as a sulfate-dominant episode, while a ratio above 1.5 was defined as a nitrate-dominant episode. When the ratio is close to 1.5, we defined it as a complex episode, which is dominated by both nitrate and sulfate. The extremely high level and contribution of K^+ and the ratio of K^+/OC are indicators of a BB episode (Duan et al., 2004; Wang et al., 2015; Zhou et al., 2017). Both K^+ and Cl^- exhibit remarkably high concentrations and proportions during the Spring Festival (Chinese New Year) due to the fireworks displays (Feng et al., 2012; Tian et al., 2017).

3.4.1. Sulfate dominated episode

The formation of sulfate is due to the homogeneous gas-phase oxidation of SO_2 by OH radicals. In addition to homogeneous reactions, sulfate can also be formed by the heterogeneous reaction on the particle surfaces (Sun et al., 2006; Wang et al., 2006; Wang et al., 2018c). Previous studies suggested that the heterogeneous reaction is correlated with a high RH and gas-phase oxidation is closely related to T (Li et al., 2017; Sun et al., 2006).

In this study, the SOR shows a good correlation with O_3 ($R^2 = 0.84$ and 0.93) and T ($R^2 = 0.81$ and 0.84) during Ep2 and Ep5, respectively. The O_3 commonly serves as an indicator of photochemical processes (Zheng et al., 2015). Such results indicate that Ep2 and Ep5 might be dominated by gas-phase oxidation to form sulfate. Furthermore, the RH was lower than 60% in Ep2 and constant under dry conditions (RH < 60%) in which sulfate existed primarily as solid phase. This is not conducive to the occurrence of aqueous phase reaction, agrees with the results of Tian et al. (2016). The Ep2 was greatly influenced by the decrease of the planetary boundary layer (PBL; Fig. 6). Zheng et al. (2015) suggested that the decrease of the PBL height hinders the vertical mixing of pollution, leading to a faster accumulation and higher level of pollutant loading. The concentration of O_3 gradually increased and reached to 91 μg m^{-3} and 74 μg m^{-3} in Ep2 and Ep5, respectively, and a large amount of solar radiation, was observed at 11:00–17:00 LST on January 5, 2014, during Ep2 and at 9:00–15:00 LST on November 22, 2014, during Ep5. Moreover, O_3 showed an obvious diurnal variation with the highest level at noon but low level in the morning and evening, which exhibited the typical characteristics of photochemical processes (Zhao et al., 2013). Hua et al. (2008) previously found that the strong photochemical reaction could be triggered during 12:00–18:00 on sunny days, which is in agreement with the present results. It was thus supposed that strong photochemical activities during Ep2 and Ep5 could lead to the generation of sufficient oxidants (OH and H_2O_2 radicals) required for gas-phase oxidation (Tian et al., 2016). Thus, the sulfate episodes during Ep2 and Ep5 were dominated by gas-phase oxidation.

Several studies showed that a fast increase in the SO_4^{2-} concentration is strongly associated with a high level of NO_2 under high RH (Li et al., 2017; Ma et al., 2018; Wang et al., 2016b). Furthermore, possible mechanisms of the heterogeneous reaction of SO_2 on dust surfaces have been proposed; mineral dust and NO_2 accelerate the conversion of SO_2 to SO_4^{2-} with a high RH and NH_3 neutralization (Li et al., 2017; Ma et al., 2018; Wang et al., 2016b). For example, Xie et al. (2015) showed in field observations in Nanjing that the formation of SO_4^{2-} was enhanced by NO_2. In this study, the RH and NO_2 concentration were high during Ep5, ranging from 76% to 99% and from 49 to 114 μg m^{-3}, respectively. Moreover, the ammonia was rich and gradually increased, reached to 18.4 μg m^{-3}, during Ep5 (Fig. S7). These conditions are beneficial for NO_2 promoting the heterogeneous conversion of SO_2 to SO_4^{2-}. To find evidence for this reaction mechanism, we compared the correlation between SO_4^{2-}, $PM_{2.5}$, SO_2, and NO_2. It was found that the NO_2, SO_2, $PM_{2.5}$ and SO_4^{2-} concentrations increase, but the increment of NO_2 is far larger than that of SO_2, leading to a high increase in SO_4^{2-} and $PM_{2.5}$ (Fig. 5b and c). The cause is the high NO_2 concentration decreasing the environmental capacity for SO_2; thus, the high level of NO_2 promotes the oxidation of SO_2 to SO_4^{2-} (Ma et al., 2018). The SO_4^{2-} concentration correlates well with $PM_{2.5}$. The $PM_{2.5}$ shows a good correlation with NO_2 ($R^2 = 0.5$) and SO_4^{2-} also exhibits a good correlation with NO_2 ($R^2 = 0.7$). With increasing NO_2 concentration, the SO_4^{2-} concentration increases the most. These results confirm that the NO_2 promotes the conversion of SO_2 to SO_4^{2-}. Accordingly, the heterogeneous reaction also plays an important role in the formation of sulfate during Ep5.

3.4.2. Nitrate dominated episode

Nitrate mainly formed through the heterogeneous reaction of nitrate radicals at nighttime and the gas-phase oxidation of NO_2 by OH during the daytime (Finlayson-Pitts et al., 2003).

During the first half stage of Ep1 and the whole Ep10, the O_3 concentration (<10 μg m^{-3}) is low, and solar radiation is weak occurred between 4:00 and 10:00 LST in the morning. The high concentration of fine particles under a low O_3 level can be attributed to the following causes. On one hand, the high level of aerosol constrains the production of O_3 because of the decrease of UV radiation, resulting in a reduced photochemical activity. On the other hand, aerosol can serve as venue for heterogeneous reactions, accompanied by the consumption of O_3 and formation of secondary aerosols. These conditions can induce the decrease in O_3 and increase in the aerosol level (Zheng et al., 2015). It was well known that the low level of O_3 and high level of NO_2 (>60 μg m^{-3}) show that the photochemical activity was weak, and sufficient OH and H_2O_2 radicals for gas-phase oxidation could not be produced (Hua et al., 2008). Zheng et al. (2015) showed that the reduced oxidation could be compensated by the increase in the aerosol volume concentrations. In addition, other oxidations, such as O_2 and organic peroxides, may be available under a high RH. Accordingly, nitrate-dominant episodes can be dominated probably by the heterogeneous reactions, rather than homogeneous gas-phase oxidation. The results show that the RH was high (>80%; Fig. 5a), which is

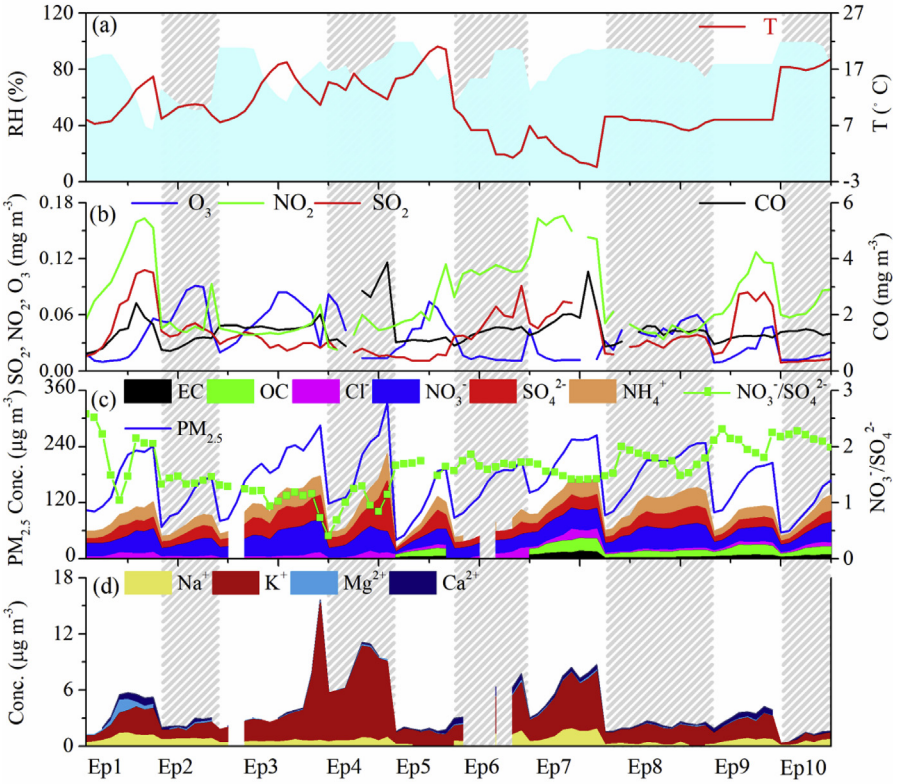

Fig. 5. Meteorological conditions (RH and T), $PM_{2.5}$, gaseous pollutants (SO_2, NO_2, O_3, and CO), and chemical $PM_{2.5}$ components during a 6 h EG episode under stagnant conditions in Shanghai in late autumn and winter from 2014 to 2017. Note that Ep1 occurred at 5:00–13:00 LST on January 3, 2014; Ep2 occurred at 11:00–17:00 LST on January 5, 2014; Ep3 occurred at 8:00–20:00 LST on January 30, 2014; Ep4 occurred from 21:00 LST on February 1 to 04:00 LST on February 2, 2014; Ep5 occurred at 9:00–15:00 LST on November 22, 2014; Ep6 occurred at 16:00 LST on December 28 to 00:00 LST on December 29, 2014; Ep7 occurred at 18:00 LST on January 10 to 2:00 LST on January 11, 2015; Ep8 occurred at 22:00 LST on December 24 to 10:00 LST on December 25, 2015; Ep9 occurred at 6:00–13:00 LST on January 2, 2016; and Ep10 occurred at 4:00–10:00 LST on November 14, 2016.

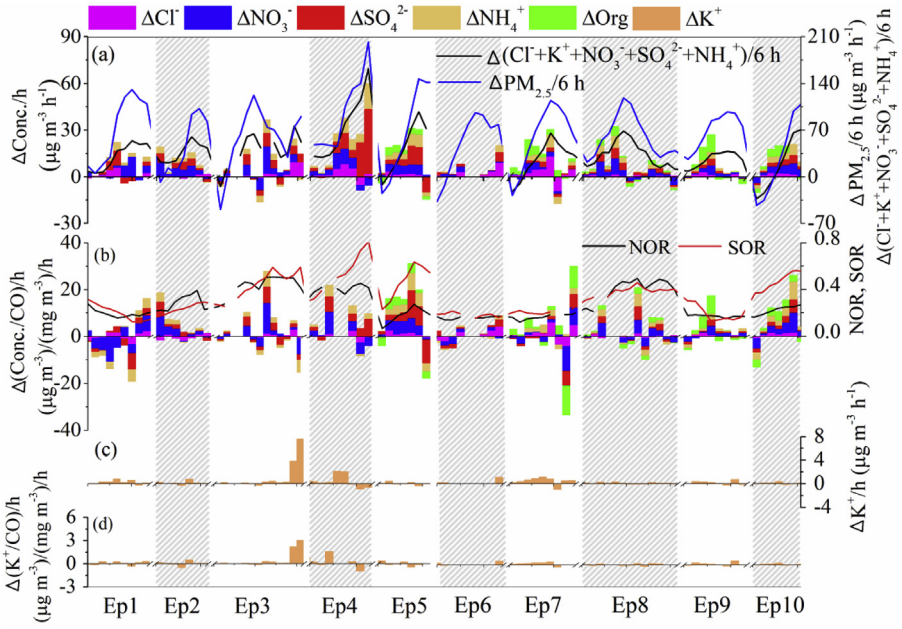

Fig. 6. Apparent growth and chemical transformation of chemical components during a 6 h EG episode under stagnant conditions in Shanghai in late autumn and winter from 2014 to 2017. (a) EG rate of chemical $PM_{2.5}$ components at 1 h, $PM_{2.5}$ and chemical $PM_{2.5}$ components at 6 h; (b) CO-scaled EG rate of chemical $PM_{2.5}$ components, SOR and NOR; (c) EG rate of K^+; and (d) CO-scaled EG rate of K^+.

favorable for heterogeneous reactions. In addition, we calculated the water content by ISORROPIA (Version 1.7, available at http://isorropia.eas.gatech.edu; Nenes et al., 1998), and found that water content of the particles ranges from 86.9 to 124.8 μg m^{-3} and from 39.7 to 118.5 μg m^{-3} during the first half stage of Ep1 and the whole Ep10, respectively. Previous studies showed that higher the water content is, the easier it is influenced by the heterogeneous reaction of NO_2 to nitrate in a high-nitrate episode (Kong et al., 2018). These results indicate that the first half stage of Ep 1 and the whole Ep10 were dominated by heterogeneous reactions.

The dominant reaction in the latter half of Ep1 differs. The equivalent concentration ratio of $[NH_4^+]$ and $[NO_3^-+SO_4^{2-}]$ during Ep1 is shown in Fig. S8a. These results show that NO_3^- and SO_4^{2-} were completely neutralized by NH_4^+, indicating that the environment was ammonium-rich. The molar ratio of $[NO_3^-]/[SO_4^{2-}]$ linearly increased with the increase in the $[NH_4^+]/[SO_4^{2-}]$ ratio (Fig. S8b). The intercept value of the linear regression line is 2.85. The excess of NH_4^+ was defined as follows: $[NH_4^+]_{excess} = ([NH_4^+]/[SO_4^{2-}] - 2.85) \times [SO_4^{2-}]$. The $[NH_4^+]_{excess}$ is always larger than 0 (Fig. S8c) and shows a good linear correlation with NO_3^- ($R^2 = 0.97$). This suggests that the homogeneous gas-phase reaction among ammonia and nitric acid is the primary source of NO_3^- (Jansen et al., 2014; Pathak et al., 2009). In addition, the O_3 level started to increase and reached 60 μg m^{-3}, accompanied by the intensification of the solar radiation, which provided sufficient OH radicals for the gas-phase oxidation. Accordingly, the latter half stage of Ep1 was dominated by a gas-phase reaction and a decrease in the PBL height.

3.4.3. Fireworks and biomass burning episodes

During the BB episode (Ep7), the mean concentration of $PM_{2.5}$ was 212 μg m^{-3}, which is 1.4 times higher than that of other EG episodes. The mean mass level of K^+ was 4.5 μg m^{-3} (it sharply increased from 2.2 to 6.1 μg m^{-3}), which is 1.7 times higher than that of other EG episodes. The contribution of K^+ to $PM_{2.5}$ was 2.1% during the BB episode, which is 1.3 times higher than that of other EG episodes. The concentration of OC during the BB episode was 22.2 μg m^{-3}, which is 1.6 times higher than that of other EG episodes and accounts for 10.4% of $PM_{2.5}$. The level of EC during the BB episode was 12.8 μg m^{-3}, which is 2.6 times higher than that of other EG episodes, contributing 6.0% to $PM_{2.5}$, which is 1.5 times higher than that of other EG episodes. Research showed that the K^+/OC ratio ranges from 0.19 to 0.21 in Beijing (Duan et al., 2004), which suggests that open BB could play a significant role in this pollution episode. The K^+/OC ratio was 0.21 during the BB episode in our study, which is in good agreement with previous studies.

The Ep4 was used to investigate a fireworks (FW) episode in this study. The mean $PM_{2.5}$ concentration during FW episodes (195.8 μg m^{-3}) was 1.3 times higher than that of other EG episodes (152.2 μg m^{-3}; Fig. 5c). This coincides with a previous study based on which the mean $PM_{2.5}$ concentration is 1.2 times higher during a FW episode than in any other haze episode (Zhang et al., 2017). The $PM_{2.5}$ concentration was lower than 255.3 μg m^{-3} in 2012 in Shanghai (Feng et al., 2012), which suggests that FW emissions are effectively controlled in Shanghai. The K^+ concentration (7.5 μg m^{-3}) sharply increased during the FW episode and was 3.3 times higher than that of other EG episodes, accounting for 4.0% of $PM_{2.5}$. The Cl^- concentration sharply increased from 1.5 μg m^{-3} to a high value of 16.0 μg m^{-3}, with an average of 7.8 μg m^{-3}, contributing 3.4% to $PM_{2.5}$.

4. Conclusions

We investigated the chemical characteristics, sources, and dominant factors of EG episodes in Shanghai in late autumn and winter from 2014 to 2017. The annual frequency and $PM_{2.5}$ concentration during each EG episode gradually decreased over the 2014–2017 period. The mean $PM_{2.5}$ level gradually decreased with increasing length of EG.

The PSCF analysis shows that the high concentrations of pollution mainly originate in East China (Zhejiang, Jiangsu, Shandong, and Anhui Province), and the NCP. The total duration, frequency, and $PM_{2.5}$ concentration during each EG episode under stagnant conditions (230 h, 26, $PM_{2.5}$: 163.0 μg m^{-3}) were slightly higher than those influenced by regional transport (198 h, 25, $PM_{2.5}$: 156.9 μg m^{-3}), which indicates that stagnant conditions played an important role in the EG episode. The dominant aerosol components of $PM_{2.5}$ were NO_3^-, OM, SO_4^{2-}, and NH_4^+ in Shanghai in late autumn and winter, contributing 17.9%, 14.1%, 13.1%, and 13.1% to $PM_{2.5}$, respectively. These results show that the secondary SNA species dominated the EG. The fastest EG rate of NO_3^- and higher ratio of NO_3^-/SO_4^{2-} under low visibility indicate that the EG episode was dominated by vehicle emissions, which underlines the importance of effective vehicle emission control in Shanghai. The EG was driven by secondary transformation (SO_4^{2-}, NO_3^-, and NH_4^+) and primary emissions (vehicle emissions, FW, and BB), but secondary transformation contributed more to the EG event. The heterogeneous and gas-phase oxidation reactions could play an important role in the sulfate-dominant and nitrate-dominant episodes. The heterogeneous reaction closely correlates with RH; however, the details of the formation mechanisms differ in each EG episode. This study enhances our understanding of the causes of EG. We recommend to pay more attention to secondary inorganic compounds, especially nitrate. Our work also provides basic data for atmospheric scientific research in Shanghai.

Acknowledgments

This work was funded by the Ministry of Science and Technology of China (No.2016YFC0202700, 2016YFE0112200), National Natural Science Foundation of China (No. 91743202, 21527814) and Marie Skłodowska-Curie Actions (690958-MARSU-RISE-2015).

Appendix A. Supplementary data

Supplementary data to this article can be found online at https://doi.org/10.1016/j.envpol.2019.07.032.

References

Arimoto, R., Duce, R., Savoie, D., Prospero, J., Talbot, R., Cullen, J., Tomza, U., Lewis, N., Ray, B., 1996. Relationships among aerosol constituents from Asia and the north Pacific during PEM-west A. J. Geophys. Res. Atmos. 101, 2011–2023.

Chang, Y., Deng, C., Cao, F., Cao, C., Zou, Z., Liu, S., Lee, X., Li, J., Zhang, G., Zhang, Y., 2017. Assessment of carbonaceous aerosols in Shanghai, China-Part 1: long-term evolution, seasonal variations, and meteorological effects. Atmos. Chem. Phys. 17, 9945–9964.

Chen, D., Cui, H., Zhao, Y., Yin, L., Lu, Y., Wang, Q., 2017. A two-year study of carbonaceous aerosols in ambient $PM_{2.5}$ at a regional background site for western Yangtze River Delta, China. Atmos. Res. 183, 351–361.

Cheng, Y., Zheng, G., Wei, C., Mu, Q., Zheng, B., Wang, Z., Gao, M., Zhang, Q., He, K., Carmichael, G., Pöschl, U., Su, H., 2016. Reactive nitrogen chemistry in aerosol water as a source of sulfate during haze events in China. Sci. Adv. 2, 1601530–1601530.

Choi, J., Heo, J., Ban, S., Yi, S., Zoh, K., 2012. Chemical characteristics of $PM_{2.5}$ aerosol in Incheon, Korea. Atmos. Environ. 60, 583–592.

Duan, F., Liu, X., Yu, T., Cachier, H., 2004. Identification and estimate of biomass burning contribution to the urban aerosol organic carbon concentrations in Beijing. Atmos. Environ. 38, 1275–1282.

Feng, J., Sun, P., Hu, X., Zhao, W., Wu, M., Fu, J., 2012. The chemical composition and sources of $PM_{2.5}$ during the 2009 Chinese New Year's holiday in Shanghai. Atmos. Res. 118, 435–444.

Finlayson-Pitts, B., Wingen, L., Sumner, A., Syomin, D., Ramazan, K., 2003. The heterogeneous hydrolysis of NO_2 in laboratory system and in outdoor and indoor atmospheres: an integrated mechanism. Phys. Chem. Chem. Phys. 5, 223–242.

Fu, H., Chen, J., 2017. Formation, features and controlling strategies of severe haze-

fog pollution in China. Sci. Total Environ. 578, 121–138.
Giorio, C., Tapparo, A., Dall'Osto, M., Beddows, D., Esser-Gietl, J., Healy, R., Harrison, R., 2015. Local and regional components of aerosol in a heavily trafficked street canyon in central London derived from PMF and cluster analysis of single-particle ATOFMS spectra. Environ. Sci. Technol. 49, 3330–3340.
Guo, S., Hu, M., Zamora, M., Peng, J., Shang, D., Zheng, J., Du, Z., Wu, Z., Shao, M., Zeng, L., Molina, M., Zhang, R., 2014. Elucidating severe urban haze formation in China. Proc. Natl. Acad. Sci. U.S.A. 111, 17373–17378.
Han, S., Wu, J., Zhang, Y., Cai, Z., Feng, Y., Yao, Q., Li, X., Liu, Y., Zhang, M., 2014. Characteristics and formation mechanism of a winter haze–fog episode in Tianjin, China. Atmos. Environ. 98, 323–330.
He, L., Chen, H., Rangognio, J., Yahyaoui, A., Colin, P., Wang, J., Daële, V., Mellouki, A., 2018. Fine particles at a background site in Central France: chemical compositions, seasonal variations and pollution events. Sci. Total Environ. 612, 1159–1170.
Hua, W., Chen, Z., Jie, C., Kondo, Y., Hofzumahaus, A., Takegawa, N., Chang, C., Lu, K., Miyazaki, Y., Kita, K., Wang, H., Zhang, Y., Hu, M., 2008. Atmospheric hydrogen peroxide and organic hydroperoxides during PRIDE-PRD'06, China: their concentration, formation mechanism and contribution to secondary aerosols. Atmos. Chem. Phys. 8, 6755–6773.
Huang, Q., Cai, X., Song, Y., Zhu, T., 2017. Air stagnation in China (1985-2014): climatological mean features and trends. Atmos. Chem. Phys. 17, 7793–7805.
Huang, R., Zhang, Y., Bozzetti, C., Ho, K., Cao, J., Han, Y., Daellenbach, K., Slowik, J., Platt, S., Canonaco, F., Zotter, P., Wolf, R., Pieber, S., Bruns, E., Crippa, M., Ciarelli, G., Piazzalunga, A., Schwikowski, M., Abbaszade, G., Schnelle-Kreis, J., Zimmermann, R., An, Z., Szidat, S., Baltensperger, U., El Haddad, I., Prevot, A., 2014. High secondary aerosol contribution to particulate pollution during haze events in China. Nature. 514, 218–222.
Jansen, R., Shi, Y., Chen, J., Hu, Y., Xu, C., Hong, S., Li, J., Zhang, M., 2014. Using hourly measurements to explore the role of secondary inorganic aerosol in $PM_{2.5}$ during haze and fog in Hangzhou, China. Adv. Atmos. Sci. 31, 1427–1434.
Ji, D., Li, L., Wang, Y., Zhang, J., Cheng, M., Sun, Y., Liu, Z., Wang, L., Tang, G., Hu, B., Chao, N., Wen, T., Miao, H., 2014. The heaviest particulate air-pollution episodes occurred in northern China in January, 2013: insights gained from observation. Atmos. Environ. 92, 546–556.
Ji, Y., Qin, X., Wang, B., Xu, J., Shen, J., Chen, J., Huang, K., Deng, C., Yan, R., Xu, K., Zhang, T., 2018. Counteractive effects of regional transport and emission control on the formation of fine particles: a case study during the Hangzhou G20 summit. Atmos. Chem. Phys. 18, 13581–13600.
Kong, L., Du, C., Zhanzakova, A., Cheng, T., Yang, X., Wang, L., Fu, H., Chen, J., Zhang, S., 2018. Trends in heterogeneous aqueous reaction in continuous haze episodes in suburban Shanghai: an in-depth case study. Sci. Total Environ. 634, 1192–1204.
Leng, C., Duan, J., Xu, C., Zhang, H., Wang, Y., Wang, Y., Li, X., Kong, L., Tao, J., Zhang, R., Cheng, T., Zha, S., Yu, X., 2016. Insights into a historic severe haze event in Shanghai: synoptic situation, boundary layer and pollutants. Atmos. Chem. Phys. 16, 9221–9234.
Li, G., Bei, N., Cao, J., Huang, R., Wu, J., Feng, T., Wang, Y., Liu, S., Zhang, Q., Tie, X., Molina, L., 2017. A possible pathway for rapid growth of sulfate during haze days in China. Atmos. Chem. Phys. 17, 3301–3316.
Li, J., Han, Z., 2016. A modeling study of severe winter haze events in Beijing and its neighboring regions. Atmos. Res. 170, 87–97.
Li, L., An, J., Zhou, M., Yan, R., Huang, C., Lu, Q., Lin, L., Wang, Y., Tao, S., Qiao, L., Zhu, S., Chen, C., 2015. Source apportionment of fine particles and its chemical components over the Yangtze River Delta, China during a heavy haze pollution episode. Atmos. Environ. 123, 415–429.
Ma, J., Chu, B., Liu, J., Liu, Y., Zhang, H., He, H., 2018. NOx promotion of SO_2 conversion to sulfate: an important mechanism for the occurrence of heavy haze during winter in Beijing. Environ. Pollut. 233, 662–669.
Nenes, A., Pandis, S., Pilinis, C., 1998. ISORROPIA: a new thermodynamic equilibrium model for multiphase multicomponent inorganic aerosols. Aquat. Geochem. 4, 123–152.
Pathak, R., Wu, W., Wang, T., 2009. Summertime $PM_{2.5}$ ionic species in four major cities of China: nitrate formation in an ammonia-deficient atmosphere. Atmos. Chem. Phys. 9, 1711–1722.
Polissar, A., Hopke, P., Paatero, P., Kaufmann, Y., Hall, D., Bodhaine, B., Dutton, E., Harris, J., 1999. The aerosol at Barrow, Alaska: long-term trends and source locations. Atmos. Environ. 33, 2441–2458.
Sun, Y., Zhuang, G., Tang, A., Wang, Y., An, Z., 2006. Chemical characteristics of $PM_{2.5}$ and PM_{10} in haze-fog episodes in Beijing. Environ. Sci. Technol. 40, 3148–3155.
Tan, J., Duan, J., He, K., Ma, Y., Duan, F., Chen, Y., Fu, J., 2009. Chemical characteristics of $PM_{2.5}$ during a typical haze episode in Guangzhou. Environ. Sci. 21, 774–781.
Tao, J., Zhang, L., Gao, J., Wang, H., Chai, F., Wang, S., 2015. Aerosol chemical composition and light scattering during a winter season in Beijing. Atmos. Environ. 110, 36–44.
Tao, J., Zhang, L., Cao, J., Zhong, L., Chen, D., Yang, Y., Chen, D., Chen, L., Zhang, Z., Wu, Y., Xia, Y., Ye, S., Zhang, R., 2017. Source apportionment of $PM_{2.5}$ at urban and suburban areas of the Pearl River Delta region, south China-with emphasis on ship emissions. Sci. Total Environ. 574, 1559–1570.
Tian, M., Wang, H., Chen, Y., Yang, F., Zhang, X., Zou, Q., Zhang, R., Ma, Y., He, K., 2016. Characteristics of aerosol pollution during heavy haze events in Suzhou, China. Atmos. Chem. Phys. 16, 7357–7371.
Tian, M., Wang, H., Chen, Y., Zhang, L., Shi, G., Liu, Y., Yu, J., Zhai, C., Wang, J., Yang, F., 2017. Highly time-resolved characterization of water-soluble inorganic ions in $PM_{2.5}$ in a humid and acidic mega city in Sichuan Basin, China. Sci. Total. Environ. 580, 224–234.
Wang, D., Zhou, B., Fu, Q., Zhao, Q., Zhang, Q., Chen, J., Yang, X., Duan, Y., Li, J., 2016a. Intense secondary aerosol formation due to strong atmospheric photochemical reactions in summer: observations at a rural site in eastern Yangtze River Delta of China. Sci. Total Environ. 571, 1454–1466.
Wang, G., Zhang, R., Gomez, M., Yang, L., Levy Zamora, M., Hu, M., Lin, Y., Peng, J., Guo, S., Meng, J., Li, J., Cheng, C., Hu, T., Ren, Y., Wang, Y., Gao, J., Cao, J., An, Z., Zhou, W., Li, G., Wang, J., Tian, P., Marrero-Ortiz, W., Secrest, J., Du, Z., Zheng, J., Shang, D., Zeng, L., Shao, M., Wang, W., Huang, Y., Wang, Y., Zhu, Y., Li, Y., Hu, J., Pan, B., Cai, L., Cheng, Y., Ji, Y., Zhang, F., Rosenfeld, D., Liss, P., Duce, R., Kolb, C., Molina, M., 2016b. Persistent sulfate formation from London Fog to Chinese haze. Proc. Natl. Acad. Sci. U. S. A. 113, 13630–13635.
Wang, G., Zhang, F., Peng, J., Duan, L., Ji, Y., Marrero-Ortiz, W., Wang, J., Li, J., Wu, C., Cao, C., Wang, Y., Zheng, J., Secrest, J., Li, Y., Wang, Y., Li, H., Li, N., Zhang, R., 2018a. Particle acidity and sulfate production during severe haze events in China cannot be reliably inferred by assuming a mixture of inorganic salts. Atmos. Chem. Phys. 18, 10123–10132.
Wang, H., Peng, Y., Zhang, X., Liu, H., Zhang, M., Che, H., Cheng, Y., Zheng, Y., 2018b. Contributions to the explosive growth of $PM_{2.5}$ mass due to aerosol-radiation feedback and decrease in turbulent diffusion during a red alert heavy haze in Beijing-Tianjin-Hebei, China. Atmos. Chem. Phys. 18, 17717–17733.
Wang, H., Tian, M., Chen, Y., Shi, G., Liu, Y., Yang, F., Zhang, L., Deng, L., Yu, J., Peng, C., Cao, X., 2018c. Seasonal characteristics, formation mechanisms and source origins of $PM_{2.5}$ in two megacities in Sichuan Basin, China. Atmos. Chem. Phys. 18, 865–881.
Wang, Q., Zhuang, G., Huang, K., Liu, T., Deng, C., Xu, J., Lin, Y., Guo, Z., Chen, Y., Fu, Q., Fu, J., Chen, J., 2015. Probing the severe haze pollution in three typical regions of China: characteristics, sources and regional impacts. Atmos. Environ. 120, 76–88.
Wang, X., Chen, J., Sun, J., Li, W., Yang, L., Wen, L., Wang, W., Wang, X., Collett, J., Shi, Y., Zhang, Q., Hu, J., Yao, L., Zhu, Y., Sui, X., Sun, X., Mellouki, A., 2014a. Severe haze episodes and seriously polluted fog water in Ji'nan, China. Sci. Total Environ. 493, 133–137.
Wang, Y., Zhuang, G., Sun, Y., An, Z., 2006. The variation of characteristics and formation mechanisms of aerosols in dust, haze, and clear days in Beijing. Atmos. Environ. 40, 6579–6591.
Wang, Y., Yao, L., Wang, L., Liu, Z., Ji, D., Tang, G., Zhang, J., Sun, Y., Hu, B., Xin, J., 2014b. Mechanism for the formation of the January 2013 heavy haze pollution episode over central and eastern China. Sci. China Earth Sci. 57, 14–25.
Xie, Y., Ding, A., Nie, W., Mao, H., Qi, X., Huang, X., Xu, Z., Kerminen, V., Petaja, T., Chi, X., Virkkula, A., Boy, M., Xue, L., Guo, J., Sun, J., Yang, X., Kulmala, M., Fu, C., 2015. Enhanced sulfate formation by nitrogen dioxide: implications from in situ observations at the sorpes station. J. Geophys. Res. Atmos. 120, 12679–12694.
Xu, J., Wang, Q., Deng, C., McNeill, V., Fankhauser, A., Wang, F., Zheng, X., Shen, J., Huang, K., Zhuang, G., 2018. Insights into the characteristics and sources of primary and secondary organic carbon: high time resolution observation in urban Shanghai. Environ. Pollut. 233, 1177–1187.
Ye, Z., Liu, J., Gu, A., Feng, F., Liu, Y., Bi, C., Xu, J., Li, L., Chen, H., Chen, Y., Dai, L., Zhou, Q., Ge, X., 2017. Chemical characterization of fine particulate matter in Changzhou, China, and source apportionment with offline aerosol mass spectrometry. Atmos. Chem. Phys. 17, 2573–2592.
Zhang, B., Wang, Y., Hao, J., 2015. Simulating aerosol–radiation–cloud feedbacks on meteorology and air quality over eastern China under severe haze conditions in winter. Atmos. Chem. Phys. 15, 2387–2404.
Zhang, Y., Wei, J., Tang, A., Zheng, A., Shao, Z., Liu, X., 2017. Chemical characteristics of $PM_{2.5}$ during 2015 Spring Festival in Beijing, China. Aerosol. Air Qual. Res. 17, 1169–1180.
Zhao, M., Huang, Z., Qiao, T., Zhang, Y., Xiu, G., Yu, J., 2015. Chemical characterization, the transport pathways and potential sources of $PM_{2.5}$ in Shanghai: seasonal variations. Atmos. Res. 158, 66–78.
Zhao, X., Zhao, P., Xu, J., Meng, W., Pu, W., Dong, F., He, D., Shi, Q., 2013. Analysis of a winter regional haze event and its formation mechanism in the North China Plain. Atmos. Chem. Phys. 13, 5685–5696.
Zheng, G., Duan, F., Su, H., Ma, Y., Cheng, Y., Zheng, B., Zhang, Q., Huang, T., Kimoto, T., Chang, D., Pöschl, U., Cheng, Y., He, K., 2015. Exploring the severe winter haze in Beijing: the impact of synoptic weather, regional transport and heterogeneous reactions. Atmos. Chem. Phys. 15, 2969–2983.
Zhong, J., Zhang, X., Dong, Y., Wang, Y., Liu, C., Wang, J., Zhang, Y., Che, H., 2018. Feedback effects of boundary-layer meteorological factors on cumulative explosive growth of $PM_{2.5}$ during winter heavy pollution episodes in Beijing from 2013 to 2016. Atmos. Chem. Phys. 18, 247–258.
Zhong, J., Zhang, X., Wang, Y., Wang, J., Shen, X., Zhang, H., Wang, T., Xie, Z., Liu, C., Zhang, H., Zhao, T., Sun, J., Fan, S., Gao, Z., Li, Y., Wang, L., 2019. The two-way feedback mechanism between unfavorable meteorological conditions and cumulative aerosol pollution in various haze regions of China. Atmos. Chem. Phys. 19, 3287–3306.
Zhou, S., Yang, L., Gao, R., Wang, X., Gao, X., Nie, W., Xu, P., Zhang, Q., Wang, W., 2017. A comparison study of carbonaceous aerosols in a typical North China Plain urban atmosphere: seasonal variability, sources and implications to haze formation. Atmos. Environ. 149, 95–103.